Int. J. Nano Dimens., 6(5): 487-500, 2015 (Special Issue for NCNC, Dec. 2014, IRAN)
DOI: 10.7508/ijnd.2015.05.006

Research Paper

Estimation of pull-in instability voltage of Euler-Bernoulli micro beam by back propagation artificial neural network

M. Heidari *

Mechanical Engineering Group, Aligudarz Branch, Islamic Azad University, Aligudarz, Iran

Received 20 February 2015; revised 12 July 2015; accepted 20 July 2015; available online 21 August 2015

ABSTRACT: The static pull-in instability of beam-type micro-electromechanical systems is theoretically investigated. Two engineering cases including cantilever and double cantilever micro-beam are considered. Considering the mid-plane stretching as the source of the nonlinearity in the beam behavior, a nonlinear size-dependent Euler-Bernoulli beam model is used based on a modified couple stress theory, capable of capturing the size effect. By selecting a range of geometric parameters such as beam lengths, width, thickness, gaps and size effect, we identify the static pull-in instability voltage. Back propagation artificial neural network with three functions have been used for modeling the static pull-in instability voltage of the micro cantilever beam. The network has four inputs of length, width, gap and the ratio of height to scale parameter of the beam as the independent process variables, and the output is static pull-in voltage of microbeam. Numerical data, employed for training the network and capabilities of the model in predicting the pull-in instability behavior has been verified. The output obtained from the neural network model is compared with numerical results, and the amount of relative error has been calculated. Based on this verification error, it is shown that the back propagation neural network has the average error of 6.36% in predicting pull-in voltage of the cantilever micro-beam.

Keywords: *Artificial neural networks; Euler-Bernoulli; Modified couple stress theory; Nonlinear micro-beam; Static pull-in instability.*

INTRODUCTION

Micro-electromechanical systems (MEMS) are widely being used in today's technology. So investigating the problems referring to MEMS, owns a great importance. One of the significant fields of study is the stability analysis of the parametrically excited systems. Parametrically excited micro-electromechanical devices are ever increasingly being used in radio, computer and laser engineering [1]. Parametric excitation occurs in a wide range of mechanics, due to time dependent excitations, especially periodic ones; some examples are columns made of nonlinear elastic material, beams with a harmonically variable length, parametrically excited pendulums and so forth. Investigating stability analysis of parametrically excited MEM systems is of great importance. In 1995 Gasparini *et al.* [2] studied on the transition between the stability and instability of a cantilevered beam exposed to a partially follower load. Applying voltage difference between an electrode and ground causes the electrode to deflect towards the ground. At a critical voltage, which is known as a pull-in voltage, the electrode becomes unstable and pulls-in onto the substrate. The pull-in behavior of MEMS actuators has been studied for over two decades without considering the casimir force [3–5]. Osterberg *et al.* [3, 4] investigated the pull-in parameters of the beam-type and circular MEMS actuators using the distributed parameter models. Sadeghian *et al.* [5] applied the generalized differential quadrature method to investigate the pull-in phenomena of micro-switches. A comprehensive literature review on investigating MEMS actuators can be found in Ref. [6]. Further information about modeling pull-in instability of MEMS has been presented in Ref. [7, 8]. The classical continuum mechanics theories are not capable of prediction and explanation of the size-dependent behaviors which occur in micron- and sub-micron-scale structures. However, some non-classical continuum

*Corresponding Author: Mohammad Heidari
Email: *moh104337@yahoo.com*
Tel.: (+98) 9131835779
Fax: (+98) 3833343096

theories such as higher-order gradient theories and the couple stress theory have been developed such that they are acceptably able to interpret the size-dependencies. In the 1960s, some researchers such as Koiter [9], Mindlin [10] and Toupin [11] introduced the couple stress elasticity theory as a non-classic theory capable to predict the size effects with the appearance of two higher-order material constants in the corresponding constitutive equations. In this theory, beside the classical stress components acting on elements of materials, the couple stress components, as higher-order stresses, are also available which tend to rotate the elements. Utilizing the couple stress theory, some researchers investigated the size effects in some problems [12].Employing the equilibrium equation of moments of couples beside the classical equilibrium equations of forces and moments of forces, a modified couple stress theory introduced by Yang, Chong, Lam, and Tong [13], with one higher-order material constant in the constitutive equations. Recently, size-dependent nonlinear Euler–Bernoulli and Timoshenko beams modeled on the basis of the modified couple stress theory have been developed by Xia *et al.* [14], and Asghari *et al.* [15], respectively. Rong *et al.* [16] present an analytical method for pull-in analysis of clamped–clamped multilayer beam. Their method is Rayleigh-Ritz method and assumes one deflection shape function. They derive the two governing equations by enforcing the pull-in conditions that the first and second order derivatives of the system energy functional are zero. In their model, the pull-in voltage and displacement are coupled in the two governing equations.

This paper investigates the pull-in instability of micro-beams with a curved ground electrode under the action of electric field force within the framework of von-Karman nonlinearity and the Euler–Bernoulli beam theory. The static pull-in voltage instability of clamped-clamped and cantilever micro-beam are obtained by using MAPLE commercial software. The effects of geometric parameters such as beam lengths, width, thickness, gaps and size effect are discussed in detail through a numerical study. The objective of this paper is to establish a neural network model for estimating the pull-in instability voltage of cantilever beams. More specifically, back propagation neural network is used to construct the pull-in instability voltage. Effective parameters influencing pull-in voltage and their levels of training were selected through preliminary calculations carried out on instability pull-in voltage of micro-beam. The network trained by the same numerical data are then verified by some numerical calculations different from those used in the training phase, and the best model was selected based on the criterion of having the least average values of verification errors. To the authors' best knowledge, no previous studies which cover all these issues are available. To the authors' best knowledge, no previous studies which cover all these issues are available.

EXPERIMENTAL

Preliminaries

In the modified couple stress theory, the strain energy density $\overline{u}$ of a linear elastic isotropic material in infinitesimal deformation is written as [17]:

$$\overline{u} = \frac{1}{2}(\sigma_{ij}\varepsilon_{ij} + m_{ij}\chi_{ij}) \quad (i, j = 1,2,3) \tag{1}$$

Where

$$\sigma_{ij} = \lambda\varepsilon_{mm}\delta_{ij} + 2\mu\varepsilon_{ij} \tag{2}$$

$$\varepsilon_{ij} = \frac{1}{2}((\nabla u)_{ij} + (\nabla u)_{ij}^{T}) \tag{3}$$

$$m_{ij} = 2l^{2}\mu\chi_{ij} \tag{4}$$

$$\chi_{ij} = \frac{1}{2}((\nabla\theta)_{ij} + (\nabla\theta)_{ij}^{T}) \tag{5}$$

In which σ_{ij}, ε_{ij}, m_{ij} and χ_{ij} denote the components of the symmetric part of stress tensor σ, the strain tensor ε, the deviatoric part of the couple stress tensor m and the symmetric part of the curvature tensor χ, respectively. Also, u and θ are the displacement vector and the rotation vector. The two Lame constants and the material length scale parameter are represented by λ, μ and l, respectively. The Lame constants are written in terms of the Young's modulus E and the Poisson's ratio ν as $\lambda = \nu E/(1+\nu)(1-2\nu)$ and $\mu = E/2(1+\nu)$. The components of the infinitesimal rotation vector θ_i relate to the components of the displacement vector field u_i as [18]:

$$\theta_i = \frac{1}{2}(curl\,(u))_i \tag{6}$$

For an Euler–Bernoulli beam, the displacement field can be expressed as:

$$u_x = u(x,t) - z\frac{\partial w(x,t)}{\partial x},\ u_y = 0,\ u_z = w(x,t) \tag{7}$$

Where *u* is the axial displacement of the centroid of sections, and *w* denotes the lateral deflection of the beam. The parameter $\partial w/\partial x$ stands in the angle of rotation (about the y-axis) of the beam cross-sections. Assuming the above displacement field, after deformation, the cross sections remain plane and always perpendicular to the center line, without any change in their shapes. It is noted that parameter z represents the distance of a point on the section with respect the axis parallel to y-direction passing through the centroid.

Governing Equation of Motion

In this section, the governing equation and corresponding classical and non-classical boundary conditions of a nonlinear microbeam modeled on the basis of the couple stress theory are derived. The coordinate system and loading of an Euler–Bernoulli beam has been depicted in Fig. 1. In this figure, *F(x,t)* and *G(x,t)* refer to the intensity of the transverse distributed force and the axial body force, respectively, both as force per unit length.

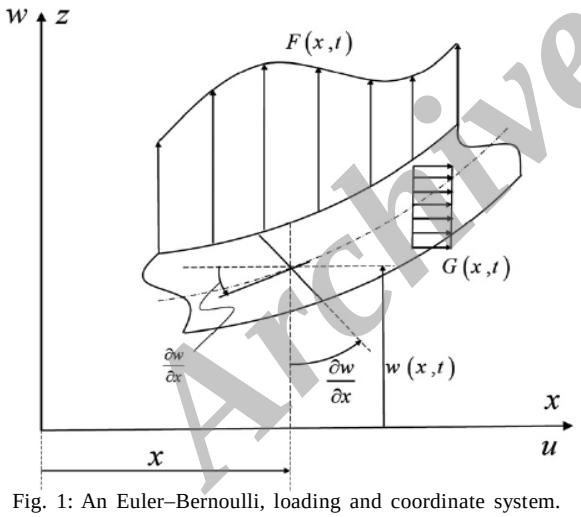

Fig. 1: An Euler–Bernoulli, loading and coordinate system.

By assuming small slopes in the beam after deformation, the axial strain, i.e. the ratio of the elongation of a material line element initially in the axial direction of its initial length, can be approximately expressed by the von-Karman strain as:

$$\varepsilon_{xx} = \frac{\partial u_x}{\partial x} + \frac{1}{2}(\frac{\partial w}{\partial x})^2 = \frac{\partial u}{\partial x} - z\frac{\partial^2 w}{\partial x^2} + \frac{1}{2}(\frac{\partial w}{\partial x})^2 \qquad (8)$$

It is noted that finite deflection w is permissible and only it is needed that the slopes be very small. Hereafter, we use Eq. (8) for the axial strain, instead of the infinitesimal definition presented in Eq. (3). Substitution of Eqs. (7) and (8) into (3)–(5) yields the non-zero components.

Also, combination of Eqs. (6) and (7) gives [19]:

$$\theta_y = -\frac{\partial w}{\partial x}, \theta_x = \theta_z = 0 \qquad (9)$$

Substitution of Eq. (9) into (5) yields the following expression for the only non-zero components of the symmetric curvature tensor:

$$\chi_{xy} = \chi_{yx} = -\frac{1}{2}\frac{\partial^2 w}{\partial x^2} \qquad (10)$$

It is assumed that the components of strains, rotations and their gradients are sufficiently small. By neglecting the Poisson's effect, the substitution of Eq. (8) into Eq. (2) gives the following expressions for the main components of the symmetric part of the stress tensor in terms of the kinematic parameters:

$$\sigma_{xx} = E\varepsilon_{xx} = E(\frac{\partial u}{\partial x} - z\frac{\partial^2 w}{\partial x^2} + \frac{1}{2}(\frac{\partial w}{\partial x})^2), \text{ all other } \sigma_{ij} = 0 \qquad (11)$$

Where *E* denotes the elastic modulus. In order to write the non-zero components of the deviatoric part of the couple stress tensor in terms of the kinematic parameters, one can substitute Eq. (10) into Eq. (4) to get:

$$m_{xy} = -\mu l^2 \frac{\partial^2 w}{\partial x^2} \qquad (12)$$

Where μ and *l* are shear modulus and the material length scale parameter, respectively. To obtain the governing equations, the kinetic energy of the beam *T*, the beam strain energy due to bending and the change of the stretch with respect to the initial configuration U_{bs}, and the increase in the stored energy with respect to the initial configuration due to the existence of initially axial load U_{is} and finally the total potential energy $U = U_{bs} + U_{is}$ are considered as follows:

$$T = \frac{1}{2}\int_0^L \int_A \rho\{(\frac{\partial u}{\partial t} - z\frac{\partial^2 w}{\partial t \partial x})^2 + (\frac{\partial w}{\partial t})^2\} dA\, dx \qquad (13a)$$

$$U = \frac{1}{2}\int_0^L \{EI(\frac{\partial^2 w}{\partial x^2})^2 + EA(\frac{\partial u}{\partial x} + \frac{1}{2}(\frac{\partial w}{\partial x})^2)^2 + \\ + N_0[2\frac{\partial u}{\partial x} + (\frac{\partial w}{\partial x})^2] + \frac{\mu A l^2}{2}(\frac{\partial^2 w}{\partial x^2})\}dx \quad (13b)$$

Where N_0, I and ρ are the axial load, area moment of inertia of the section about y– axis and the mass density, respectively. The work done by the external loads acting on the beam is also expressed as:

$$\delta W = \int_0^L F(x,t)\delta w\, dx + \int_0^L G(x,t)\,\delta u\, dx \\ + (\hat{N}\,\delta u)\Big|_{x=0}^{x=L} + (\hat{V}\,\delta w)\Big|_{x=0}^{x=L} + (\hat{M}\,\delta(\frac{\partial w}{\partial x}))\Big|_{x=0}^{x=L} \quad (13c) \\ + (\hat{P}^h\,\delta(\frac{\partial u}{\partial x} + \frac{1}{2}(\frac{\partial w}{\partial x})^2)\Big|_{x=0}^{x=L} + (\hat{Q}^h\,\delta(\frac{\partial^2 w}{\partial x^2}))\Big|_{x=0}^{x=L}$$

Where $\hat{N}$ and $\hat{V}$ represent the resultant axial and transverse forces in a section caused by the classical stress components acting on the section. The resultant axial and transverse forces are work conjugate to u and w, respectively. Also, $\hat{P}^h$ and $\hat{Q}^h$ are the higher-order resultants in a section, caused by higher-order stresses acting on the section. These two higher-order resultants are work conjugate to $\varepsilon_{xx} = \partial u/\partial x + 1/2(\partial w/\partial x)^2$ and $\partial^2 w/\partial x^2$, respectively. The parameter $\hat{M}$ is the resultant moment in a section caused by the classical and higher-order stress components. Now, the Hamilton principle can be applied to determine the governing equation:

$$\int_{t_1}^{t_2}(\delta T - \delta U + \delta W)dt = 0 \quad (14)$$

Where δ denotes the variation symbol. By applying Eqs. (13) and (14), the governing equilibrium micro beam is derived as:

$$S\frac{\partial^4 w}{\partial x^4} - N\frac{\partial^2 w}{\partial x^2} + \rho A\frac{\partial^2 w}{\partial t^2} = F(x,t) \quad (15)$$

Where

$$N = N_0 + \frac{EA}{2L}\int_0^L (\frac{\partial w}{\partial x})^2 dx \quad (16)$$

$$S = EI + \mu A l^2 \quad (17)$$

If in Eq. (15), *N=0*, then the model the of beam is called the linear equation (linear model) without the effect of geometric nonlinearity. The cross sectional area and length of beam are *A* and *L* respectively. *F(x,t)* is the electrostatic force per unit length of the beam. The electrostatic force enhanced with first order fringing correction can be presented in the following equation [20]:

$$F_{elec}(x,t) = \frac{\varepsilon_0 B V^2}{2(g-w)^2}[1 + 0.65\frac{(g-w)}{B}] \quad (18)$$

Where $\varepsilon_0 = 8.854\times10^{-12}\, C^2 N^{-1} m^{-2}$ is the permittivity of vacuum, *V* is the applied voltage, *g* is the initial gap between the movable and the ground electrode and *B* is the width of the beam. For clamped-clamped beam, the boundary conditions at the ends are:

$$w(0) = 0,\ \frac{dw(0)}{dx} = 0;\ \ w(L) = 0,\ \frac{dw(L)}{dx} = 0 \quad (19)$$

For cantilever beam, the boundary conditions at the ends are:

$$w(0) = 0,\ \frac{dw(0)}{dx} = 0;\ \frac{d^2 w(L)}{dx^2} = 0,\ \frac{d^3 w(L)}{dx^3} = 0 \quad (20)$$

Table 1 shows the geometrical parameters and material properties of micro-beam.

Table 1: Geometrical parameters and material properties of micro-beam

Material properties		Geometrical dimensions			
E(GPa)	ν	L (μm)	B(μm)	h(μm)	g (μm)
77	0.33	100-500	0.5-50	0.5-4	0-30

In the static case, we have $\frac{\partial}{\partial \tau} = 0$ and $\frac{\partial}{\partial x} = \frac{d}{dx}$. Hence, Eq. (15) is reduced to:

$$(EI + \mu A l^2)\frac{d^4 w}{dx^4} - [N_0 + \frac{EA}{2L}\int_0^L (\frac{dw}{dx})^2 dx]\frac{d^2 w}{dx^2} = \\ = \frac{\varepsilon_0 B V^2}{2(g-w)^2}[1 + 0.65\frac{(g-w)}{B}] \quad (21)$$

A uniform micro-beam has a rectangular cross section with height *h* and width *B*, subjected to a given electrostatic force per unit length. Let us consider the following dimensionless parameters:

$$\alpha = \frac{AL^2}{2I},\ \beta = \frac{\varepsilon_0 B V^2 L^4}{2g^3 EI},\ \gamma = 0.65\frac{g}{B},\ \delta = \\ \frac{\mu A l^2}{EI},\ \tilde{w} = \frac{w}{g},\ \tilde{x} = \frac{x}{L},\ \Gamma = \frac{N_0 L^2}{EI} \quad (22)$$

In the above equations, the non-dimensional parameter, δ is defined the size effect parameter. Also, β is non-dimensional voltage parameter. The normalized nonlinear governing equation of motion of the beam can be written as [21]:

$$(1+\delta)\frac{d^4\tilde{w}}{d\tilde{x}} - \{\Gamma + \alpha\int_0^1 (\frac{d\tilde{w}}{d\tilde{x}})^2 d\tilde{x}\}\frac{d^2\tilde{w}}{d\tilde{x}^2} = \frac{\beta}{(1-\tilde{w})^2} + \frac{\gamma\beta}{(1-\tilde{w})} \quad (23)$$

Artificial neural networks

Artificial NNs are non-linear mapping systems with a structure loosely based on principles observed in biological nervous systems. In greatly simplified terms as can be seen from Fig. 2, a typical real neuron has a branching dendritic tree that collects signals from many other neurons in a limited area; a cell body that integrates collected signals and generates a response signal (as well as manages metabolic functions); and a long branching axon that distributes the response through contacts with dendritic trees of many other neurons. The response of each neuron is a relatively simple non-linear function of its inputs and is largely determined by the strengths of the connections from its inputs. In spite of the relative simplicity of the individual units, systems containing many neurons can generate complex and interesting behaviours [22].

Fig. 2: A biological nervous systems.

An ANN shown in Fig. 3 is very loosely based on these ideas. In the most general terms, a NN consists of large number of simple processors linked by weighted connections. By analogy, the processing nodes may be called neurons. Each node output depends only on information that is locally available at the node, either stored internally or arriving via the weighted connections. Each unit receives inputs from many other nodes and transmits its output to yet other nodes. By itself, a single processing element is not very powerful; it generates a scalar output with a single numerical value, which is a simple non-linear function of its inputs. The power of the system emerges from the combination of many units in an appropriate way.

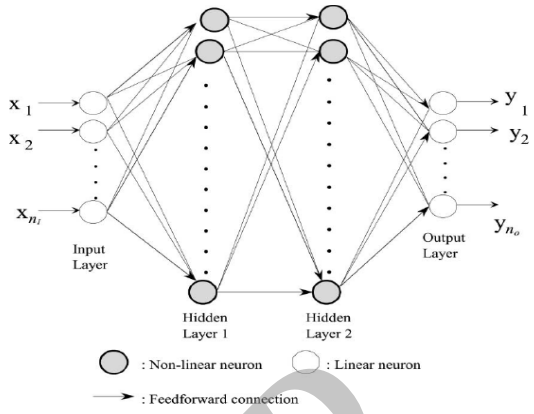

Fig. 3: A layered feed-forward artificial NN.

A network is specialized to implement different functions by varying the connection topology and the values of the connecting weights. Complex functions can be implemented by connecting units together with appropriate weights. In fact, it has been shown that a sufficiently large network with an appropriate structure and property chosen weights can approximate with arbitrary accuracy any function satisfying certain broad constraints. Usually, the processing units have responses like (see Fig. 4).

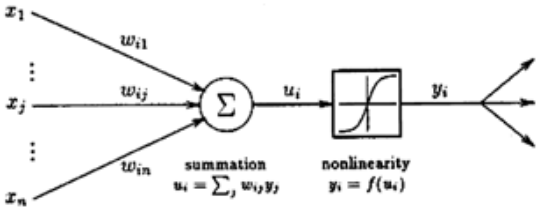

Fig. 4: an artificial neuron model.

$$y = f(\sum_i u_i) \quad (24)$$

Where, u_i are the output signals of hidden layer to the output layer, $f(u_i)$ is a simple non-linear function such as the sigmoid, or logistic function. This unit computes a weighted linear combination of its inputs and passes this through the non-linearity to produce a scalar output.

In general, it is a bounded non-decreasing non-linear function; the logistic function is a common choice. This model is, of course, a drastically simplified approximation of real nervous systems. The intent is to capture the major characteristics important in the information processing functions of real networks without varying too much about physical constraints

imposed by biology. The impressive advantages of NNs are the capability of solving highly non-linear and complex problems and the efficiency of processing imprecise and noisy data. Mainly, there are three types of training condition for NNs; namely supervised training, graded training and self-organization training. Supervised training, which is adopted in this study, can be applied as:
(1) First, the dataset of the system, including input and output values, is established;
(2) The dataset is normalized according to the algorithm;
(3) Then, the algorithm is run;
(4) Finally, the desired output values corresponding to the input used in test phase [23].

Back propagation neural network

Back propagation neural network (BPN), developed by Rumelhart [24], is the most prevalent of the supervised learning models of ANN. BPN used the gradient steepest descent method to correct the weight of the interconnectivity neuron. BPN easily solved the interaction of processing elements by adding hidden layers. In the learning process BPN, the interconnective the weights are adjusted using an error convergence technique to obtain a desired output for a given input. In general, the error at the output layer in the BPN model propagates backward to the input layer through the hidden layer in the network to obtain the final desired output. The gradient descent method is utilized to calculate the weight of the network and adjusts the weight of interconnectives to minimize the output error. The formulas used in this algorithm are as follows:
1) Hidden layer calculation results:

$$net_i = \sum x_i w_i \tag{25}$$

$$y_i = f(net_i) \tag{26}$$

Where x_i and w_i are input data and weights of the input data, respectively. f is activation function, and y_i is the result obtained from hidden layer.
2) Output layer calculation results:

$$net_k = \sum y_i w_{jk} \tag{27}$$

$$o_k = f(net_k) \tag{28}$$

Where w_{jk} are the weights of output layers, and O_k is result obtained from output layer.
3) Activation functions used in layers are logsig, tansig and linear:

$$f(net_i) = \frac{1}{1+e^{-net_i}} \quad \text{(logsig)} \tag{29}$$

$$f(net_i) = \frac{1-e^{-net_i}}{1+e^{-net_i}} \quad \text{(tansig)} \tag{30}$$

$$f(net_i) = net_i \quad \text{(linear)} \tag{31}$$

(4) Errors made at the end of one cycle:

$$e_k = (t_k - o_k) o_k (1 - o_k) \tag{32}$$

$$e_i = y_i (1 - y_i) \sum e_k w_{ij} \tag{33}$$

Where t_k is result expected from output layer, e_k is an error occurred at output layer, and e_i is the error occurred at hidden layer.
5) Weights can be changed using these calculated error values according to Eqs. (34) and (35).

$$w_{jk} = w_{jk} + \alpha e_k y_i + \beta \Delta w_{jk} \tag{34}$$

$$w_{ij} = w_{ij} + \alpha e_i x_i + \beta \Delta w_{ij} \tag{35}$$

Where w_{ij} are the weights of the output layer. Δw_{jk} and Δw_{ij} are correction made in weights at the previous calculation. α is learning ratio, and β is momentum term, that is used to adjust the weights. In this paper, $\alpha = 0.9$ and $\beta = 0.9$, are used.
2) Square error, occurred in one cycle, can be found by Eq. (36).

$$e = \sum 0.5 |t_k - o_k|^2 \tag{36}$$

The completion of training the BPN, relative error (RE) for each data and mean relative error (MRE) for all data is calculated according to Eqs. (37) and (38), respectively.

$$RE = \left(\frac{100\ (t_k - o_k)}{t_k} \right) \tag{37}$$

$$MRE = \frac{1}{n} \sum_{i=1}^{n} \left(\frac{100 (t_k - o_k)}{t_k} \right) \tag{38}$$

Where *n* is the number of data [25].

RESULTS AND DISCUSSION

Static pull-in instability analysis

When the applied voltage between the two electrodes increases beyond a critical value, the electric field force cannot be balanced by the elastic restoring force of the movable electrode and the system collapses onto the ground electrode. The voltage and deflection at this state are known as the pull-in voltage and pull-in deflection, which are of utmost importance in the design of MEMS devices.

The pull-in voltage of cantilever and fixed-fixed beams is an important variable for analysis and design of micro-switches and other micro-devices. Typically, the pull-in voltage is a function of geometry variable such as length, width, and thickness of the beam and the gap between the beam and the ground plane. To study the instability of the nano-actuator, Eq. (23) is solved numerically and simulated. To highlight the differences between linear and nonlinear geometry model results of Euler-Bernoulli micro beam, we first compare the pull-in voltage for a fixed-fixed and cantilever beams with a length of 100 μm , a width of 50, a thickness of 1 and two gap lengths. For a small gap length of 0.5 (shown in Fig. 5), we observe that linear and nonlinear geometry model gives identical results.

However, for a large gap length of 2 μm (shown in Fig. 6), we observe that pull-in voltage for fixed-fixed beam is significantly different.

As shown in Fig. 7, the difference in the pull-in voltage is even larger when a gap length of 4.5 μm is considered. In Figs. 8, 9 and 10, pull-in voltage of fixed-free beams are shown. It is evident that pull-in voltage of fixed-fixed beam is larger than fixed-free beam. More extensive studies for the cantilever beam with lengths varying from 100 to 500 and thicknesses varying from 1 to 4are shown in Figs. 11 and 12. The gap lengths used vary from 5 to 30. For gaps smaller than 15 and lengths larger than 350, we observe that the pull-in voltage obtained with linear and nonlinear geometry model are very close. However, for large gaps (such as the 15 case) and for short beams (such as the 100 case), we observe that the difference in the pull-in voltage obtained with linear and nonlinear geometry model is not negligible. In Figs. 13-14, we investigate the fixed-fixed beam example with lengths varying from 100 to 500 and thickness varying from 0.5 to 2. We observe that, for all cases, the pull-in voltage obtained with linear model are in significant error (larger than 5.5%) compared to the pull-in voltages obtained with nonlinear geometry model. When the gap increase, the error in the pull-in voltage with linear model increase significantly. Furthermore, contrary to the case of cantilever beams, the thickness has a significant effect on the error in the pull-in voltages.

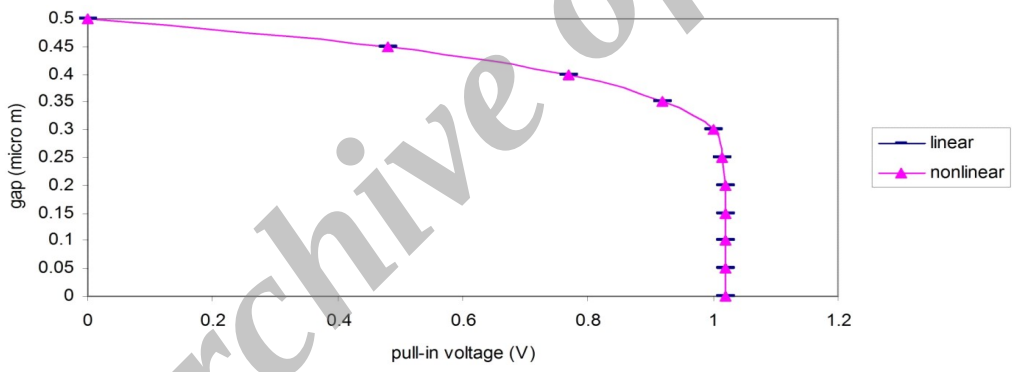

Fig. 5: Comparison of linear and nonlinear geometry model results for a fixed-fixed beam with a gap 0.5 μm .

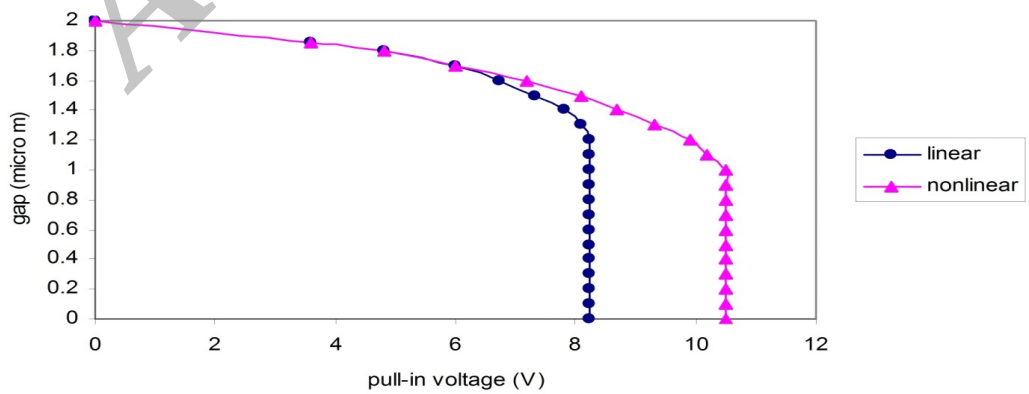

Fig. 6: Comparison of linear and nonlinear geometry model results for a fixed-fixed beam with a gap 2 μm .

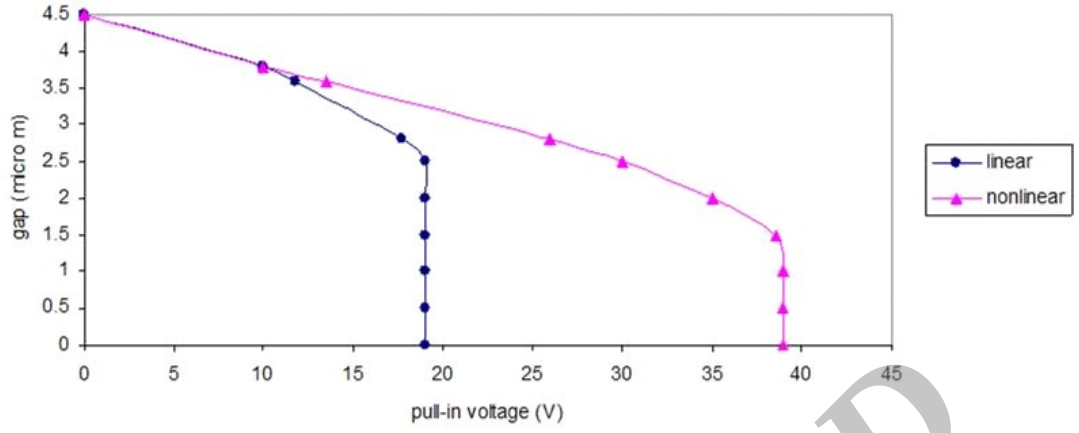

Fig. 7: Comparison of linear and nonlinear geometry model results for a fixed-fixed beam with a gap 4.5 μm .

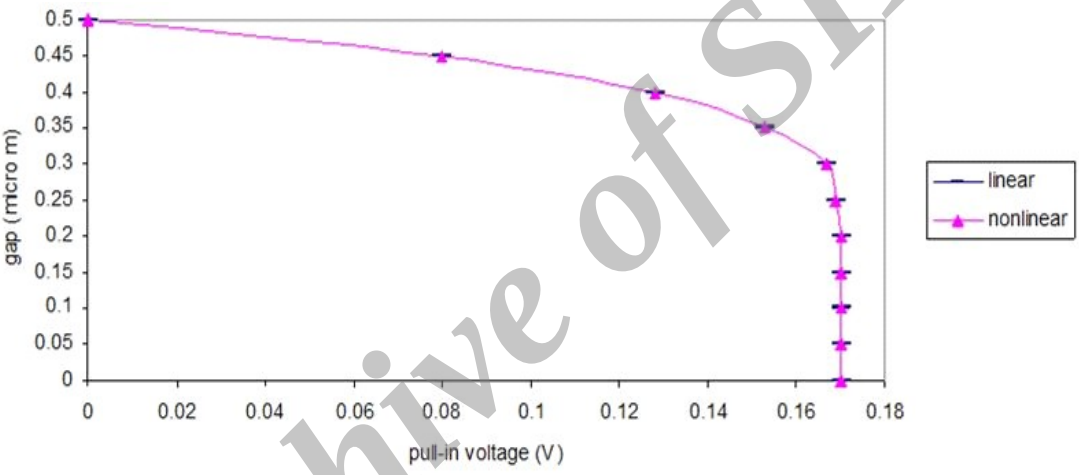

Fig. 8: Comparison of linear and nonlinear geometry model results for a fixed-free beam with a gap 0.5 μm .

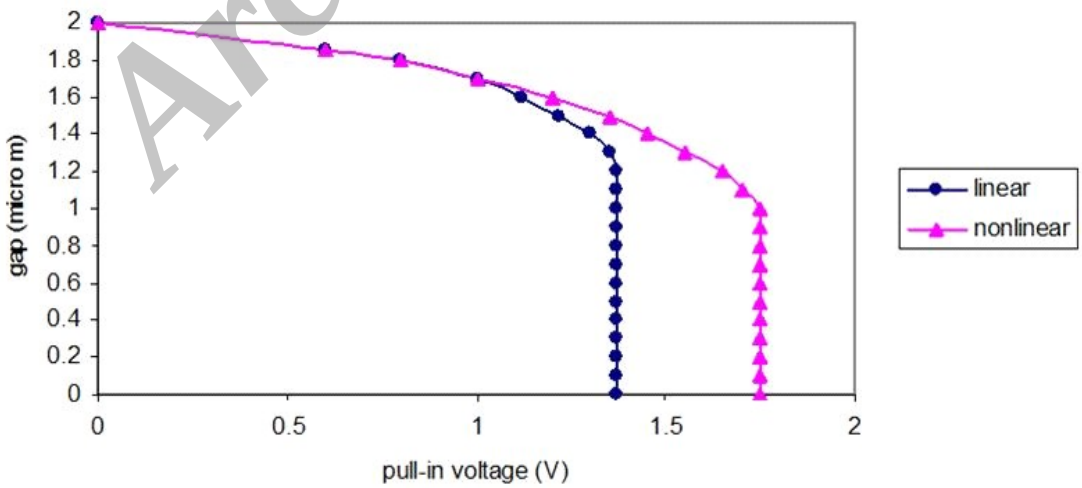

Fig. 9: Comparison of linear and nonlinear geometry model results for a fixed-free beam with a gap 2 μm .

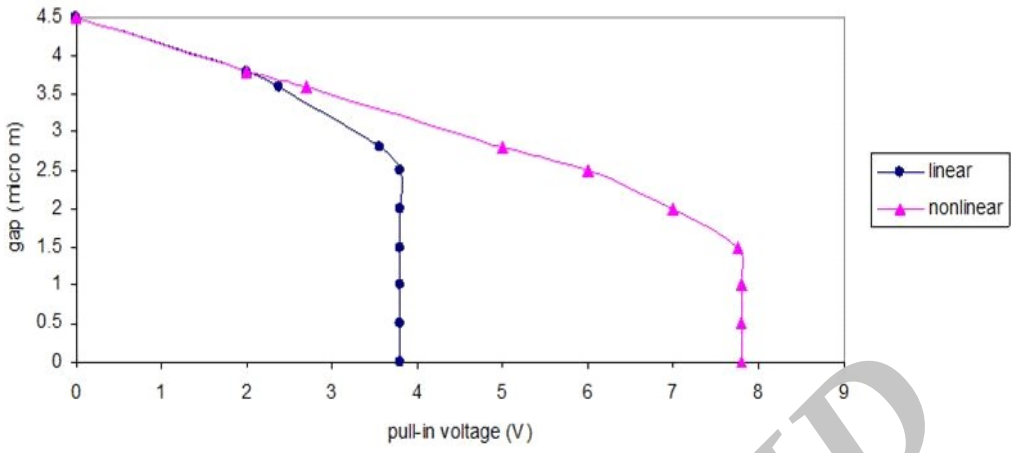

Fig. 10: Comparison of linear and nonlinear geometry model results for a fixed-free beam with a gap 4.5 μm .

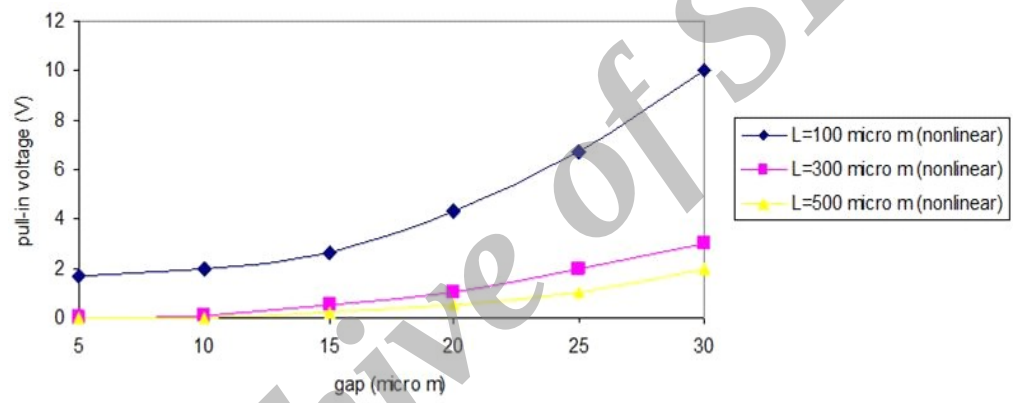

Fig. 11: Gap vs. pull-in voltage for cantilever beams with a thickness of 1 μm . For length=100 μm , the difference in pull-in voltage between linear and nonlinear geometry model is significant when the gap is larger than 15 μm . For a length larger than 350 μm , the pull-in voltages obtained with linear and nonlinear geometry model are identical.

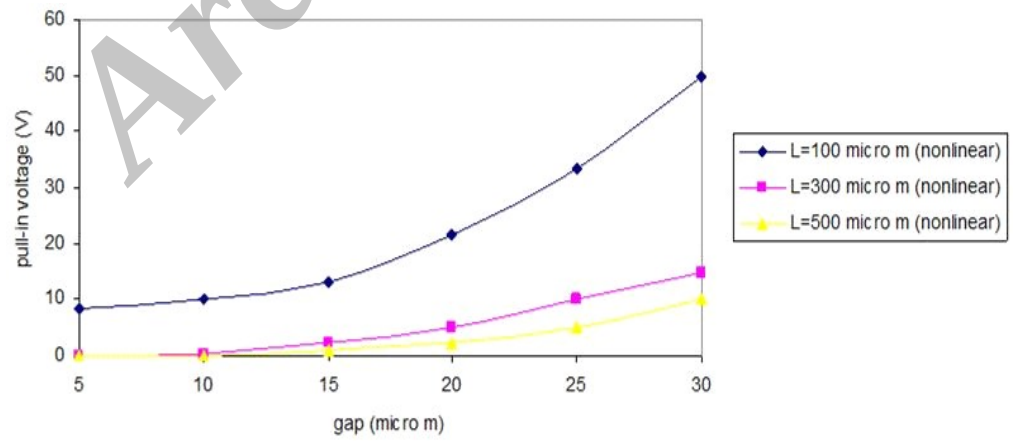

Fig. 12: Gap vs. pull-in voltage for cantilever beams with a thickness of 4 μm . For length=100 μm , the difference in pull-in voltage between linear and nonlinear geometry model is significant when the gap is larger than 15 μm . For a length larger than 350 μm , the pull-in voltages obtained with linear and nonlinear geometry model are identical.

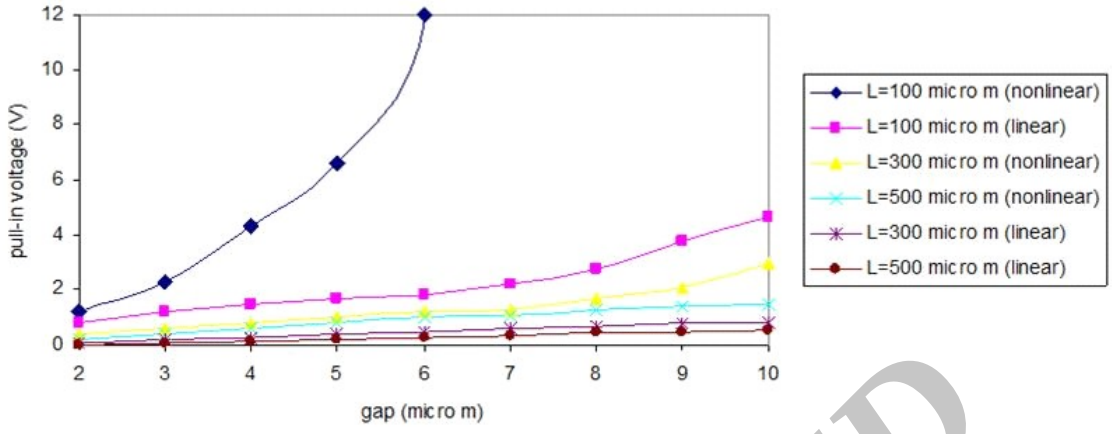

Fig. 13: Gap vs. pull-in voltage for fixed-fixed beams with a thickness of 0.5 μm. Observe the large difference in pull-in voltage obtained from linear and nonlinear geometry model of beam.

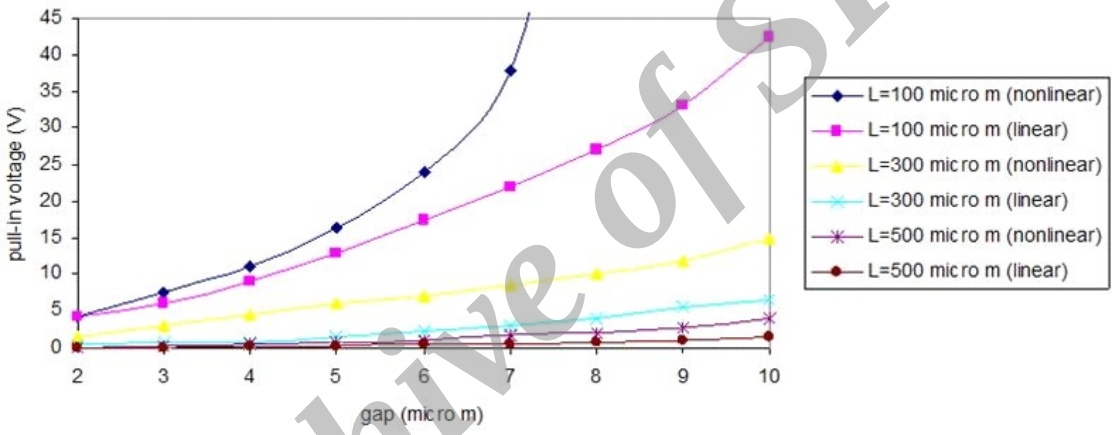

Fig. 14: Gap vs. pull-in voltage for fixed-fixed beams with a thickness of 2 μm.

The thinner the beam, the larger the error. Another observation is that the length of the beam has little effect on the error in the pull-in voltage. This observation is also different from the case of cantilever beams. From the results, it is clear the linear model is generally not valid for the fixed-fixed beams case, except when the gap is very small, such as the 0.5 case as shown in Fig. 5. These figures represent that the size effect increases the pull-in voltage of the nano-actuators. Fig. 15 shows the pull-in voltage vs. size effect for the fixed-fixed beam with gap 2.5.

Modeling of Static Pull-in Instability Voltage of Cantilever Beam Using Back Propagation Neural Network

Modeling of pull-in instability of micro-beam with BP neural network is composed of two stages: training and testing of the networks with numerical data. The training data consisted of values for beam length (L), gap (g), width of beam (b) and (h/l), and the corresponding static pull-in instability voltage (V_{PI}). total 120 such data sets were used, of which 110 were selected randomly and used for training purposes whilst the remaining 10 data sets were presented to the trained networks as new application data for verification (testing) purposes. Thus, the networks were evaluated using data that had not been used for training. Training/ Testing pattern vectors are formed, each formed with an input condition vector, and the corresponding target vector. Mapping each term to a value between -1 and 1 using the following linear mapping formula:

$$N = \frac{(R - R_{\min}) * (N_{\max} - N_{\min})}{(R_{\max} - R_{\min})} + N_{\min} \qquad (39)$$

where, N : normalized value of the real variable; $N_{\min} = -1$ and $N_{\max} = 1$: minimum and maximum values of normalization, respectively; R: real value of the variable; $R_{\min}$ and $R_{\max}$: minimum and maximum values of the real variable, respectively. These normalized data were used as the inputs and output to train the ANN. In other words, the network has four inputs of beam length (*L*), gap (*g*), width of beam (*b*) and (*h*/*l*) ratio and one output of static pull-in voltage (V_{PI}). Fig. 16 shows the general network topology for modeling the process. Table 2 shows 10 numerical data sets, have been used for verifying or testing network capabilities in modeling the process.

Therefore, the general network structure is supposed to be 4-n-1, which implies 4 neurons in the input layer, n neurons in the hidden layer, and 1 neuron in the output layer. Then, by varying the number of hidden neurons, different network configurations are trained, and their performances are checked. For training problem, equal learning rate and momentum constant of $\eta = \alpha = 0.9$ were used [25]. Also, error stopping criterion was set at *E=0.01*, which means training epochs continued until the mean square error fell beneath this value.

BP Neural Network Model

The size of hidden layer(s) is one of the most important considerations when solving actual problems using multi-layer feed-forward network. However, it has been shown that BP neural network with one hidden layer can uniformly approximate any continuous function to any desired degree of accuracy given an adequate number of neurons in the hidden layer and the correct interconnection weights [26]. Therefore, one hidden layer was adopted for the BP model. To determin the number of neurons in the hidden layer, a procedure of trail and error approach needs to be done. As such, attempts have been made to study the network performance with a different number of hidden neurons. Hence, a number of candidate networks are constructed, each of trained separately, and the "best" network were selected based on the accuracy of the predictions in the testing phase. It should be noted that if the number of hidden neurons is too large, the ANN might be over-trained giving spurious values in the testing phase. If too few neurons are selected, the function mapping might not be accomplished due to under-training. Three functions, namely newelm, newff and newcf [27] have been used for creating of BP networks. Then, by varying the number of hidden neurons, different network configurations are trained, and their performances are checked. The results are shown in Table 3. Both the required iteration numbers and mapping performances were examined for these networks. As the error criterion for all networks was the same, their performances are comparable. As a result, from Table 3, the best network structure of BP model is picked to have 8 neurons in the hidden layer with the average verification errors of 6.36% in predicting V_{PI} by newelm function.

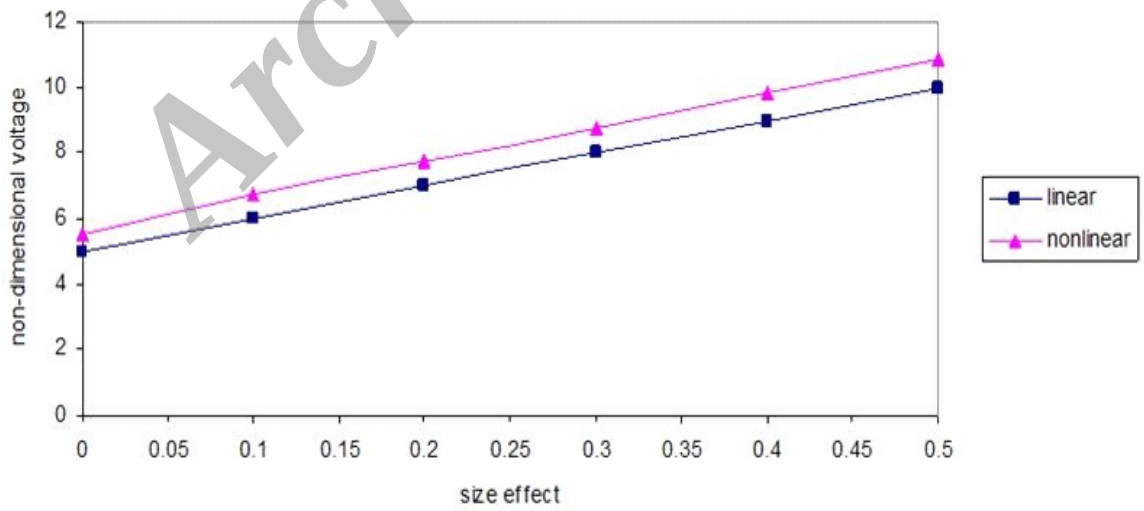

Fig. 15: Pull-in voltage vs. size effect for fixed-fixed beam with gap 2.5 μm, a thickness of 1 μm, length 300 μm and width 0.5 μm, for nonlinear geometry model.

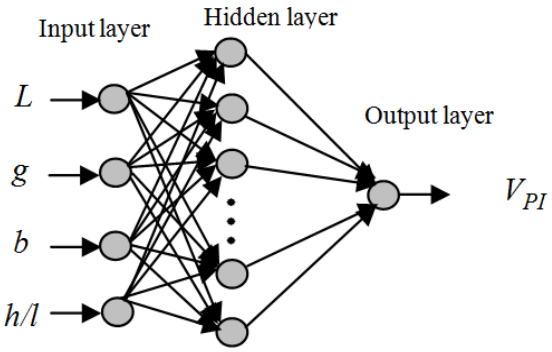

Fig. 16: General ANN topology.

Table 2: Beam geometry and pull-in voltage for verification analysis.

Test No.	L (μm)	b (μm)	h/l	g (μm)	V_{PI} (volt)
1	75	0.5	4	0.5	0.179
2	100	5	6	1	2.44
3	125	10	8	1.5	7.31
4	150	20	10	2	16.82
5	175	25	12	2.5	26.78
6	200	30	14	3	40.27
7	225	35	16	3.5	53.84
8	250	40	18	4	68.01
9	275	45	20	4.5	84.53
10	300	50	22	5	103.62

Table 3: The effects of different number of hidden neurons on the BP network performance.

No. of hidden neurons	Epoch	Average error in V_{PI} (%) with newelm function	Average error in V_{PI} (%) with newcf function	Average error in V_{PI} (%) with newff function
4	18914	12.31	10.27	12.30
5	4970	14.38	18.38	20.19
6	1783	8.19	11.65	12.75
7	3984	9.72	9.39	11.17
8	1884	6.36	8.28	10.14
9	2770	13.39	11.86	19.98
10	2683	11.67	16.40	15.48

Table 4 shows the comparison of calculated and predicted values for static pull-in voltage in verification cases. After 1884 epochs, the MSE between the desired and actual outputs becomes less than 0.01. At the beginning of the training, the output from the network is far from the target value. However, the output slowly and gradually converges to the target value with more epochs and the network learns the input/output relation of the training samples. Fig. 17 shows the pull-in voltage evaluated by the modified couple stress theory respect to length of the beam and with $h/l = 4$, $g=1.05\,\mu m$, $b=50\,\mu m$ *and* $h=2.94$. The pull-in voltage of the micro-cantilever versus parameter h/l for $b/g=50$ is depicted in Fig. 18, with three BP functions.

Table 4: Comparison of V_{PI} calculated and predicted by the BP neural network model with three functions.

Test No.	V_{PI} (volt)			V_{PI} (volt)			V_{PI} (volt)		
	Calculated	BP model (newelm)	Error (%)	Calculated	BP model (newff)	Error (%)	Calculated	BP model (newcf)	Error (%)
1	0.179	0.190	6.56	0.179	0.191	7.12	0.179	0.193	8.29
2	2.44	2.61	7.28	2.44	2.52	3.39	2.44	2.59	6.28
3	7.31	7.32	0.16	7.31	7.54	3.16	7.31	7.70	5.39
4	16.82	19.21	14.24	16.82	18.29	8.75	16.82	19.21	14.24
5	26.78	28.22	5.39	26.78	28.16	5.19	26.78	28.76	7.41
6	40.27	42.17	4.74	40.27	46.03	14.31	40.27	43.99	9.25
7	53.84	57.13	6.12	53.84	57.49	6.79	53.84	57.96	7.67
8	68.01	71.60	5.29	68.01	78.39	15.27	68.01	82.14	20.78
9	84.53	89.39	5.76	84.53	86.71	2.59	84.53	92.51	9.45
10	103.62	112.03	8.12	103.62	120.53	16.32	103.62	116.74	12.67

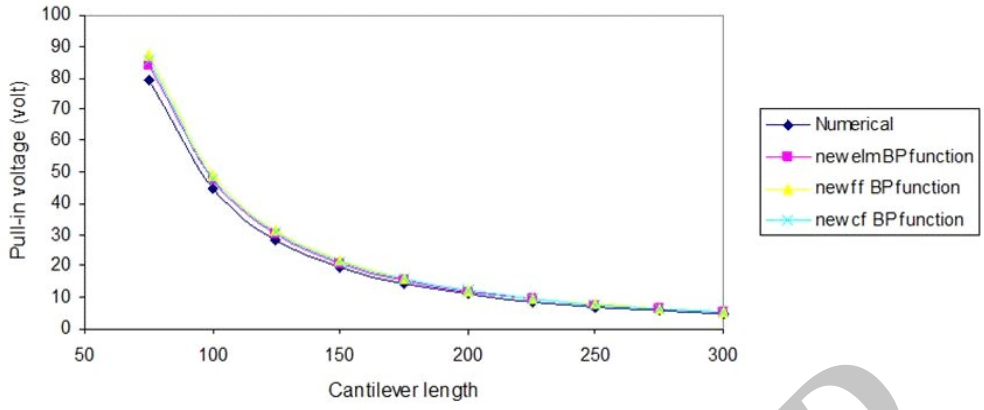

Fig. 17: Comparing the theoretical and BP neural networks pull-in voltages for silicon 110.

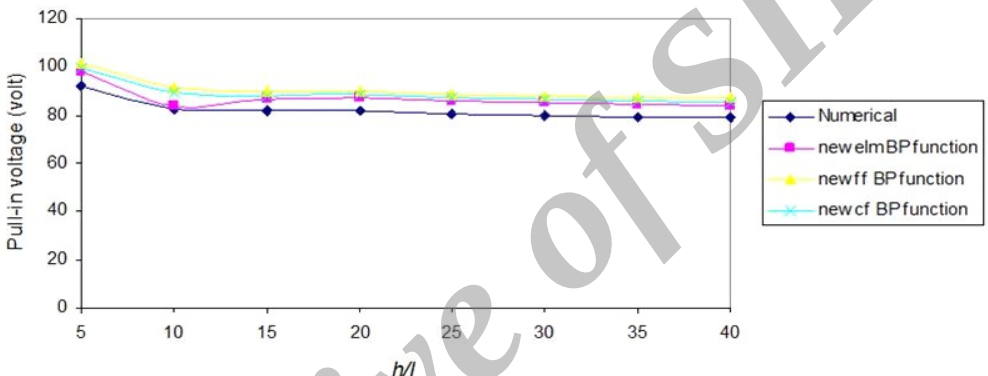

Fig. 18: Comparing of pull-in voltage of the micro-cantilever versus parameter *h/l* and *b/g=50* with BP models.

CONCLUSION

The primary contributions of the paper are summarized as follows. The BP neural network is capable of constructing model using only numerical data, describing the static pull-in instability behavior. The results show that newelm function is more accurate than newff and newcf functions. Also the Levenberg-Marquardt training is faster than other training methods. For cantilever beams, length has a significant effect on the error in pull-in voltages, while for fixed-fixed beams, the length has little effect on the error. On the other hand, for fixed-fixed beams, thickness has significant effect on the error in pull-in voltage, while for cantilever beams it has little effect. The static pull-in instability voltage of clamped–clamped and cantilever beam are compared. For both clamped–clamped and cantilever beams, the pull-in voltage in nonlinear geometry beam model is bigger than linear model. For both fixed-fixed and cantilever beams by increasing of gap length, the pull-in voltage is significantly increased. For both fixed-fixed and cantilever beams by increasing of thickness of beams, the pull-in voltage is significantly increased. For both fixed-fixed and cantilever beams by increasing of length of beams, the pull-in voltage is significantly decreased. By using modified couple stress theory, it is found that the dimensionless pull-in voltage of MEMS increases linearly due to the size effect. This emphasizes the importance of size effect consideration in design and analysis of MEMS. When the ratio of *h/l* increases, the pull-in voltage predicted by modified couple stress theory and ANN is constant approximately. The conclusion above indicates that the geometry of the beam has significant influences on the electro-static characteristics of micro-beams that can be designed to tailor for the desired performance in different MEMS applications.

REFERENCES

[1] Khatami I., Pashai M. H., Tolou N., (2008), Comparative vibration analysis of a parametrically nonlinear excited oscillator using HPM and numerical method. *Mathemat. Problems in Eng*. 2008: 1-11.

[2] Gasparini A. M., Saetta A. V., Vitaliani R. V., (1995), on the stability and instability regions of non-conservative continuous system under partially follower forces. *Comput. Meth. Appl. Mech. Eng.* 124: 63-78.

[3] Osterberg P. M., Senturia S. D., (1997), M-TEST: A test chip for MEMS material property measurements using electrostatically actuated test structures. *J. Microelectromech. Syst.* 6: 107-118.

[4] Osterberg P. M., Gupta R. K., Gilbert J. R., Senturia S. D., (1994), Quantitative models for the measurement of residual stress, poisson ratio and young's modulus using electrostatic pull-in of beams and diaphragms. Proceedings of the Solid-State Sensor and Actuator Workshop. *Hilton Head*, SC.

[5] Sadeghian H., Rezazadeh G., Osterberg P., (2007), Application of the generalized differential quadrature method to the study of pull-in phenomena of MEMS switches. *IEEE/ASME J. Micro Electro Mech. Sys.* 16: 1334-1340.

[6] Salekdeh Y. A., Koochi A., Beni Y. T., Abadyan M., (2012), Modeling effect of three nano-scale physical phenomena on instability voltage of multi-layer MEMS/NEMS: Material size dependency, van der waals force and non-classic support conditions. *Trends in Appl. Sci. Res*. 7: 1-17.

[7] Batra R. C., Porfiri M., Spinello D., (2007), Review of modeling electrostatically actuated microelectromechanical systems. *Smart Mater. Struct*. 16: R23-R31.

[8] Lin W. H., Zhao Y. P., (2008), Pull-in instability of micro-switch actuators: Model review. *Int. J. Nonlinear Sci. Numer. Simulation.* 9: 175-184.

[9] Koiter W. T., (1964), Couple-stresses in the theory of elasticity: I and II. *Proceed. Koninklijke Nederlandse Akademie van Wetenschappen Series B*. 6717-6744.

[10] Mindlin R. D., Tiersten H. F., (1962), Effects of couple-stresses in linear elasticity. *Archive for Rational Mech. Analysis.* 11: 415-448.

[11] Toupin R. A., (1962), Elastic materials with couple-stresses. *Archive for Rational Mech. Analysis*. 11: 385–414.

[12] Anthoine A., (2000), Effect of couple-stresses on the elastic bending of beams. *Int. J. Solids and Struc.* 37: 1003-1018.

[13] Yang F., Chong A. C. M., Lam D. C. C., Tong P., (2002), Couple stress based strain gradient theory for elasticity. *Int. J. Solids and Struc.* 39: 2731-2743.

[14] Xia W., Wang L., Yin L., (2010), Nonlinear non-classical microscale beams: Static bending, post buckling and free vibration. *Int. J. Eng. Sci*. 48: 2044-2053.

[15] Asghari M., Rahaeifard M., Kahrobaiyan M. H., Ahmadian M. T., (2011), On the size-dependent behavior of functionally graded micro-beams. *Mater. Design*. 32: 1435-1443.

[16] Rong H., Huang Q. A., Nie M., Li W.,(2004), An analytical model for pull-in voltage of clamped–clamped multilayer beams. *Sens. Actuators A.* 116: 15-21.

[17] Yang F., Chong A. C. M., Lam D. C. C., Tong P., (2002), Couple stress based strain gradient theory for elasticity. *Int. J. Solids and Struc.* 39: 2731-2743.

[18] Shengli K., Shenjie Z., Zhifeng N., Kai W., (2011), The size-dependent natural frequency of Bernoulli–Euler micro-beams. *J. Eng. Sci*. 46: 427-437.

[19] Ma H. M., Gao X. L., Reddy J. N., (2008), A microstructure-dependent Timoshenko beam model based on a modified couple stress theory. *J. Mech. and Physics of Solids.* 56: 3379–3391.

[20] Gupta R. K., (1997), Electrostatic pull-in test structure design for in-situ mechanical property measurements of microelectromechanical systems. Ph.D. Dissertation, Massachusetts Institute of Technology (MIT), Cambridge, MA.

[21] Zhao J., Zhou S., Wanga B., Wang X., (2012), Nonlinear microbeam model based on strain gradient theory. *Appl. Mathemat. Modell*. 36: 2674-2686.

[22] Freeman J. A., Skapura D. M., (1992), Neural networks: algorithms, applications, and programming techniques. Addision-Wesley.

[23] Gao D., Kinouchi Y., Ito K., Zhao Z., (2005), Neural networks for event extraction from time series: a back propagation algorithm approach. *Future Gener. Comp. Sys.* 21: 1096-1105.

[24] Rumelhart D. E., Hinton G. E., Williams R. J., (1986), Learning representations by back propagating error. *Nature*. 323: 533-536.

[25] Zhang H., Wei W., Mingchen Y., (2012), Boundedness and convergence of batch back-propagation algorithm with penalty for feedforward neural networks. *Neurocomputing*. 89: 141-146.

[26] Hongmei S., Gaofeng Z., (2011), Convergence analysis of a back-propagation algorithm with adaptive momentum. *Neurocomputing*. 74: 749-752.

[27] Demuth H., Beale M., (2001), Matlab Neural Networks Toolbox, User's Guide, The Math Works, Inc., *http://www.mathworks.com.*

How to cite this article: (Vancouver style)

Heidari M., (2015), Estimation of pull-in instability voltage of Euler-Bernoulli micro beam by back propagation artificial neural network. *Int. J. Nano Dimens.* 6(5): 487-500.

DOI: 10.7508/ijnd.2015.05.006

URL: http://ijnd.ir/article_15293_1117.html